MODELING AND SIMULATION OF ELECTRIC AND MAGNETIC FIELD OF A SHORT DIPOLE ANTENNA WITH LOW FREQUENCIES AT FAR FIELD.

ABSTRACT:

In this study, the electric and magnetic fields that a short dipole antenna radiates will be modeled, simulated, and their properties in the far-field regionparticularly at low frequencieswill be examined. By investigating the often-overlooked feature of radiated field characteristics, the study aims to provide a deeper knowledge of field behavior in wireless networks, where dipole antennas are often used. The study simulates the electric and magnetic fields produced at far-field distances by a dipole antenna using Python software. The link between wavelength and field strength is investigated using mathematical models that characterize the far-field behavior, which includes equations for far-field distance.The simulation takes into consideration variables like operating frequency, antenna length, and the environment in which it operates, enabling a thorough examination of the fields. The changes in the field components with greater separation from the antenna and the impact of low-frequency operation on the propagation are examined by analyzing the data. According to the calculations, when one gets farther away from the dipole antenna, there is a predictable decline in both the magnetic and electric fields. At far-field distances, the field componentsespecially the angular and radial componentsdisplay unique behaviors that are consistent with theory.

The findings demonstrate how frequency affects field distribution, with decreased frequencies resulting in longer far-field distances and a slower rate of field strength degradation. The study made clear how crucial precise modeling of the radiating fields from dipole antennas is to the efficiency of wireless communication networks. The results show that operating at low frequencies results in larger far-field zones, which may have implications for wireless system design and implementation. Engineers can guarantee higher-quality RF propagation and enhance antenna performance by comprehending these features.

Key words: Dipole antenna, Far field, Electric field, Magnetic field, Frequency, radiation pattern.

1. INTRODUCTION

Due to its simplicity and adaptability in telecommunication applications, dipole antennas—basic antennas made up of two identical metal conducting wiresare widely utilized in a variety of applications[1]. The performance of a dipole antenna depends on a number of factors, including feeding point, length, wire radius, surrounding medium, and metal conductivity. Two conducting pieces, usually rods, are fed with a sinusoidal voltage difference to form these antennas [2]. By altering the separation between the two elements, the duration of operation can be changed [3]. They are appropriate for many uses, such as RF energy harvesting, because of their flexibility [4].Dipole antennas can be improved by adding features, like p-i-n diodes for frequency reconfigurability, to this fundamental design [5].

Furthermore, because of their small size and effective impedance matching, they are also commonly employed in wireless communication [6]. The goal of recent developments has been to reduce their dimensions without sacrificing performance [7].

Characterizing the near-field and far-field areas of a dipole antenna in wireless communication situations remains a substantial research gap, despite the well-established knowledge concerning dipole antenna radiation. Comprehending the near-field to far-field transition and its constituent properties is crucial for enhancing antenna efficiency in real-world scenarios. The development of wireless communication systems, where precise far-field characterisation is crucial, is hampered by this lack of thorough research. This study analyzes a dipole antenna's field components in the far-field region using modeling and simulation approaches. We created and simulated the far-field equations. To determine correlations with

distance and other characteristics of a dipole antenna at a distance, the model's electric and magnetic fields were examined.
With the help of a thorough simulation of a dipole antenna's far-field area, the study sheds light on how the electric and magnetic fields behave in relation to the radiating source's distance. The study accurately predicts the near-field to far-field transition zone by using the far-field distance equations. In wireless communication networks, where a thorough understanding of the far-field is essential for dependable operation, this research aids in establishing ideal configurations for dipole antennas. In wireless communication, the characterisation of the near-field to far-field transition is crucial.
In order to ensure that antenna designs are optimized for practical applications and result in improved system performance, accurate modeling and understanding of the relationships between electric field, magnetic field, radiating distance, and phase angle are essential. This research fills a vacuum in the literature by concentrating on dipole antennas and the characterization of dipole antennas at low frequencies. It is strictly restricted to the modeling and simulation of far-field behavior in dipole antennas, specifically focusing on the Electric and Magnetic at far-field. The study looks at the relationships between electric and magnetic fields at low frequencies and their dependence on proximity to the antenna in wireless communication systems.

The dipole antenna is the subject of this discussion since it is a particularly significant type of RF antenna that is frequently used for radio sending and receiving applications. The dipole is a common stand-alone RF antenna, but it also serves as a key component of numerous other RF antenna designs. As a result, it may be the most significant type of RF antenna [8].

2. LITERATURE REVIEW

A review of numerous experimental examinations of dipole antenna designs has been done, showing how useful these designs are for a range of applications. It displays the usefulness, efficiency, and performance of dipole antennas in actual situations. Additionally included are the printed dipole array antenna's design, simulation, and measurement. A microstrip balun with a log-periodic frequency feeds the dipole element. The unbalanced microstrip line is transformed into a balanced two-wire line feeding the dipole by the balun. In order to design dipole arrays with two or four elements, Wilkinson power divider parallel feeding networks are used. A cheap FR4 dielectric material is used in the array design. The dielectric substrate has a height of 1.6 mm and a dielectric constant of 4.5.The electromagnetic simulator CST MWS is used to simulate the suggested antennas. For the single component, two-element, and four-element designs, respectively, the realized gains are 4.2 dB, 7.2 dB, and 9.7 dB, while the simulation-generated impedance bandwidths are 27.5%, 29.5%, and 28.6%. The array consisting of two elements has been produced and examined. There is good agreement between the measured and simulated outcomes. From modeling and measurement, the derived bandwidths are 29.5% and 27.9%, respectively. The measurement result's center frequency has been somewhat moved upward, toward 2.15GHz. The dielectric constant, which is ill-defined and can range from 4 to 5, is mostly to blame for this [9].

An investigation was carried out on a pair of dipole antennas featuring an RF beamforming circuit, intended to direct the primary beam in the azimuthal direction. A mixture of the induced EMF approach and a genetic algorithm has been successfully used to optimize the primary beam penetration from 100° to 140° with a step size of 10°. The optimization outcomes were contrasted with Empire XCCel's full-wave simulation method. The simulation and test outcomes are shown, and the design is realized practically at 2.45 GHz. The phased array antenna's measured reflection coefficient at 2.56 GHz is -48 dB. With the main beam directed at 110°, the viability of the beam synthesis has been effectively verified. Wi-Fi, wireless local area networks (WLAN), and fifth-generation indoor positioning devices can all be used with the dipole antenna system with RF beamformer circuit [10].

A 28 GHz array antenna that may be used to evaluate polarimetric omni-directional pathloss has been proposed by a researcher. A printed microstrip dipole and loop that have an integrated tapering balun structure make up the array. Wideband matching and radiation performance are demonstrated by the low profile microstrip dipole and loop antenna design and experimental findings. The dipole has attained an impedance matching bandwidth of −10 dB over 6 GHz, while the loop displays a 0.2 GHz bandwidth extending from 27.9 to 28.1 GHz. Their modeling method is validated by a rather good match between

the recorded and simulated radiation pattern. Dipole and loop antennas' omnidirectional characteristics make them appropriate for use as reference antennas in over-the-air antenna testing at 28 GHz [11].

Two tiny textile-based planar dipole and loop antennas were studied for use in 2.4 GHz industrial, scientific, and medical radio (ISM) bands wearable communication applications. The radiating structure of the antennas was created by sewing an embroidery technique onto cotton jean cloth, conducting copper threads, and a 0.44 mm thin military print. Simulations were used for the antennas' design and performance studies; additional testing in anechoic chambers and indoor environments was done to confirm the designs.
The human subjects were used in the studies, which were conducted on their torso and limb joints, in a free-space environment. Based on the reflection coefficient in both bent and normal conditions—which correspond to the various radii of the various points of the human limbs—the performance of the antennas was examined. Due to antenna bending and body effects, the antennas function well in free space and on-body situations in flat and bend settings, with return loss below −10 dB in all cases and an acceptable resonance frequency close to 2.4 GHz. This paper also reports the radiation pattern estimations for on-body and free space scenarios.The antenna radiation pattern is found to be greatly influenced by the geometry of the human body, increasing the front-to-back ratio and making the antenna more directional. Overall, it was discovered that the constructed embroidered textile antennas' performance was appropriate for a range of wearable body-centric applications in indoor settings[12].

For antenna calibration, ideal dipole antennas are preferred. However, nonideal effects are unavoidable in real-world implementation and can have a substantial impact on calibration quality. An outstanding overall performance of a 2 GHz standard dipole (SD) antenna is shown in this communication. An embedded (shielded) balun and an inventive design with an improved element form allow for the achievement of this outcome.The feeding structure that is intended is a balanced configuration that switches from coaxial to parallel strip lines. The feeding strategy achieves the right balance without being affected by the asymmetry of the electromagnetic environment. The antenna gain is roughly 2 dBi, and the dipole's measured relative bandwidth is greater than 15%. In the horizontal plane, the horizontally gain variation is beneath 0.2 dB and the cross-polarization ratio is larger than 27 dB. The greatest gain point of the dipole does not stray from the horizontal plane, and it has a symmetric vertical plane pattern. This SD is appropriate for antenna calibration due to its excellent performance [13].

Newer wireless applications require adaptable antenna designs that perform well in a variety of host configurations. An analysis of the blood irradiation applications' performance with an inkjet printed dipole antenna is provided. Antenna performance can be strongly affected by a blood environment, according to simulations and tests. Placing the dipole antenna atop a host blood bag considerably reduces its radiation pattern, with a predicted highest possible gain of −18 dBi at 2.45 GHz. The dipole antenna is merged with an AMC structure that operates at 2.45 GHz in order to separate it from the host structure.Simulations and measurements reveal significant enhancements in the antenna gain despite the existence of the lossy host. By incorporating the AMC ground plane, gains of 6.4 dBi and 4.1 dBi are obtained,respectively, in simulations and measurements [14]. It was decided to operate a folded planar dipole antenna in close proximity to the human body. In order to extend the antenna's operational range and shield the human body from undesired electromagnetic (EM) emissions, backward radiation was decreased. The idea behind the antenna design was a folded planar dipole, which has advantageous impedance bandwidth (BW) properties. The antenna was fully encased in resin for integrability and resilience when used in real-world settings, considering the trade-off between the antenna's radiation effectiveness, protection, and isolation. The measurements showed that the 2.27–2.74 GHz band was covered by a 10-dB impedance BW of 470 MHz (18.76%). At 2.45 GHz, the greatest gain was 1.4 dB isotropic (dBi). The antenna is easy to integrate with clothing because of its virtually omnidirectional pattern, small size (77 × 35 × 11.15 mm), and lightweight (120 g). Resin packaging improved the design's insulation from outside interference and disturbances and strengthened its mechanical resilience, but it decreased the efficiency of radiation to 48.35%.The proposed antenna is a great option for a variety of wireless applications, especially those that call for the antenna to endure exposure to ambient mechanical strains and electromagnetic disturbances [15]. The investigation focused on the radiation performance of a dipole antenna mounted on a three-dimensional (3D) printed diamond-structured photonic crystal (PC)

substrate that had point imperfections. In the meantime, comparable dipole antennas were constructed and bundled with conventional coaxial lines based on the PCs' reflection characteristics. Based on the experimental results, the dipole antenna's strong radiation frequency at roughly 13 GHz was found to be in basic accord with the PCs' strongest reflection frequency that had point flaws.Additionally, the experimental results demonstrate that the primary lobe's angular range was 5–55° and its maximum gain in the dipole antenna was close to −67 dB. While the primary lobe's width range was 240–270°, its maximum gain climbed to −60 dB in the composite antenna, a 7 dB improvement over the dipole antenna. These findings demonstrate how the usage of such substrates, which are based on PCs with point defects in diamond structures, could greatly increase the antenna's gain and directivity and serve as a foundation for application in engineering [16].

A researcher used Bootstrap Aggregation and Machine Learning-based Low-Scale Dipole Antenna Optimizing.With the aid of machine learning (ML) techniques, the characteristics of the dipole antenna were optimized. Experiments demonstrate how machine learning systems can explain subtle patterns in device profiles. Next, using the techniques for Linear Regression, Support Vector Regression, and Decision Tree Regression, the researcher presented a bootstrap aggregation model [17]. Characteristic Mode Assessment of Planar Dipole Antennas was studied. It involved using image theory and its dipole equivalents to analyze planar monopole antennas. the use of characteristic mode analysis to study the radiation pattern and bandwidth of planar dipoles. When the dipole width varied, a trade-off was seen between the impedance bandwidth and pattern stability. It demonstrates that modal and impedance bandwidth degradation is caused by feed point offset [18].

3.1 MATERIALS AND METHODS

3.1.1 MATERIALS

i. Laptop
ii. Python Software
iii. JupyterNoteBook

3.2 METHOD

3.2.1 SYSTEM MODEL

To determine the fields around a short dipole, we must calculate them at all points in space. Let the dipole, with length L, be aligned along the Z-axis, centered at the origin, as depicted in Figure 1. The relationships between the electric field components, E_r, E_Θ, and E_φ, are shown in the figure. It is assumed that the dipole is surrounded by air or vacuum.

When analyzing antennas or radiating systems, the propagation time is a critical factor. If a current flows through the short dipole (as illustrated in Figure 1), the impact of the current at pointPnot immediate but occurs after a delay corresponding to the time required for the disturbance to travel the distance, r. This phenomenon is referred to as the retardation effect.

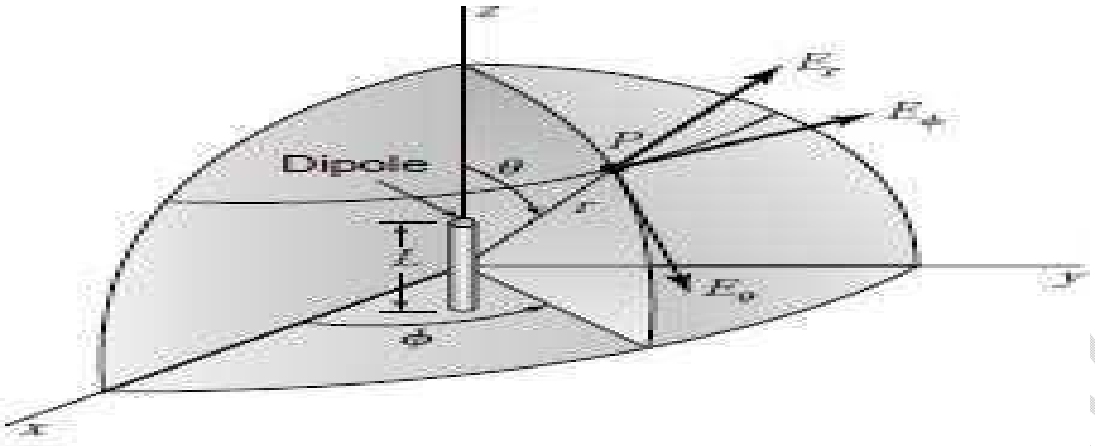

Fig.1: Relation of dipole to coordinates

Which means instantaneous propagation of the effect of the current, introducing retardation time, where I is called the retarded current. Specifically, the retardation time *r/c* results in a phase retardation

$$\frac{\omega r}{c} = 2\pi f \frac{r}{c} \text{ radians}$$

$= 360^{O} f\, r/c \;=\; 360^{O}\, t/T, t = 1/f$ = time of one period or cycle (seconds) and *f* = frequency (hertz, Hz = cycles per second).

Electric and magnetic fields can be expressed in terms of vector and scalar potentials. Therefore, to model Electric and Magnetic field, it is necessary to introduce retarded potentials since we are dealing with near and far fields, that is, *t – r/c.* For a dipole located as in Figure 1 or Figure 2, the retarded vector potential of the electric current has only one component, A_z.

Equation (3.2) is a statement of the fact that the disturbance at a time *t* and at a distance from a current element is caused by a current [*I*] that occurred at an earlier time *t – r/c*. The time difference *r/c* is the interval required for the disturbance to travel the distance r, where *c* is the velocity of light ($3*10^8$ m s^{-1}).

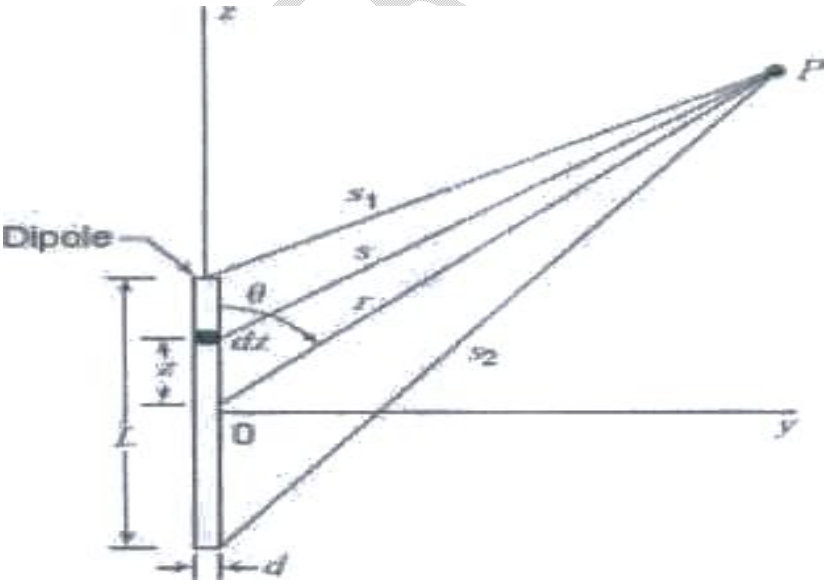

Fig.2: Geometry for short dipole

$$A_z = \frac{\mu 0}{4\pi}\int_{L/2}^{L/2}\frac{[I]}{s}dz \quad (3.1)$$

Where [I] is the retarded current given by

$$[\,\mathrm{I}] = I_0 e^{j\omega[t-(s\,/\,c)]} \quad (3.2)$$

In (3.1) and (3.2),

z= distance to a point on the conductor

I_0 = peak value in time of current (uniform along dipole)

μ_0 = permeability of free space = $4\pi \times 10^{-7}$H m^{-1}

If the distance from the dipole is large compared to its length ($r \gg L$) and if the wavelength is large compared to the length ($\lambda \gg L$), we can put s = r and neglect the phase difference of the field contributions from different parts of the wire.

The integrand in (1) can be regarded as a constant, so that (1) becomes

$$A_z = \frac{\mu_0 L I_0 e^{j\omega(t-(r\,/\,c)]}}{4\pi r} \quad (3.3)$$

The retarded scalar potential V of a charge distribution is

$$V = \frac{1}{4\pi\varepsilon_0}\int_v \frac{[\rho]}{s}d\tau \quad (3.4)$$

Where $[\rho]$ is the retarded charge density given by

$$[\rho] = \rho_0 e^{j\omega(t-(t-(s\,/\,c)]} \quad (3.5)$$

In obtaining (3.3) and (3.4), the relation was used that $\mu_0\varepsilon_0 = 1/C^2$, where C = velocity of light.

and dt = infinitesimal volume element.

ε_0 = permittivity or dielectric constant of free space = 8.85×10^{-12}F m^{-1}

Since the region of charge in the case of the dipole being considered is confined to the points as in

Figure 1, (3.4) becomes

$$V = \frac{1}{4\pi\varepsilon_0}\left\{\frac{[q\,]}{s\mathrm{I}} - \frac{[q]}{s2}\right\} \quad (3.6)$$

From (3.2),

$$[q] = \int [I]dt = I_0 \int e^{j\omega[t-(s/c)]}dt = \frac{I_0[t]}{j\omega} \tag{3.7}$$

Substituting (3.7) into (3.6),

$$V = \frac{I_0}{4\pi\varepsilon_0 j\omega}\left[\frac{e^{j\omega[s-(s1/c)]}}{s_1} - \frac{e^{j\omega[s-(s2/c)]}}{s_2}\right] \tag{3.8}$$

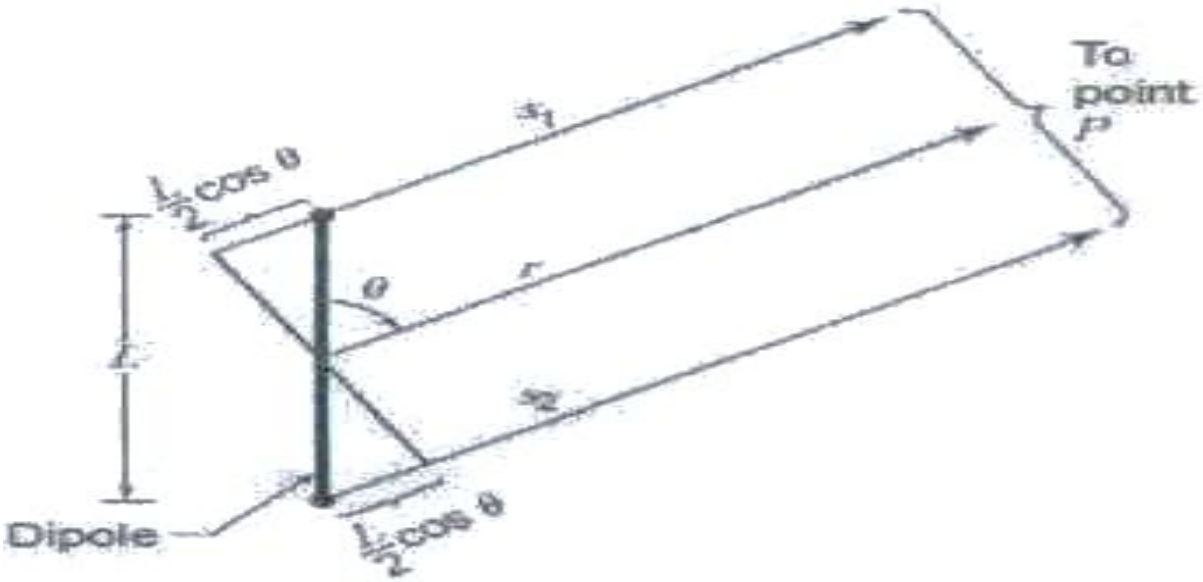

Fig.3: Geometry of Dipole ends connecting point P

Referring to Figure 3, when r ≫ L, the lines connecting the ends of the dipole and the point *P* may be considered as parallel so that

$$s_1 = r - \frac{L}{2}\cos\theta \tag{3.9}$$

and

$$s_2 = r + \frac{L}{2}\cos\theta \tag{3.10}$$

Substituting (3.9) and (3.10) into (3.8) gives Electric field of the short Dipole as

$$E_r = \frac{I_0 L\cos\theta\, e^{j\omega(t-(r/c))}}{2\pi\varepsilon_0}\left(\frac{1}{cr^2} + \frac{1}{j\omega r^3}\right) \tag{3.11}$$

$$E_\theta = \frac{I_0 L \sin\theta \, e^{j\omega(t-(r/c))}}{4\pi\varepsilon_0}\left(\frac{j\omega}{c^2 r} + \frac{1}{cr^2} + \frac{1}{j\omega r^3}\right) \quad (3.12)$$

For Magnetic field, it is calculated from curl of A such that

$$v \times A = \frac{\hat{r}}{r\sin\theta}\left[\frac{\partial(\sin\theta)A_\phi}{\partial\theta} - \frac{\partial(A_\theta)}{\partial\phi}\right] + \frac{\hat{\theta}}{r\sin\theta}\left[\frac{\partial A_r}{\partial\phi} - \frac{\partial(r\sin\theta)A_\phi}{\partial r}\right] + \frac{\hat{\phi}}{r}\left[\frac{\partial(r\,A_\theta)}{\partial r} - \frac{\partial A_r}{\partial\theta}\right] \quad (3.13)$$

Since $A\varphi$ = 0, the first and fourth terms of (3.13) are zero, since $A_r$and $A_\theta$are independent of φ, so that the second and third terms of (3.13) are also zero. So that $\nabla \times \boldsymbol{A}$,and hence also **H,** have only a φ component. Therefore, the magnetic field of short Dipole is given as;

$$[H] = H_\phi = \frac{I_0 L \cos\theta \, e^{j\omega[t-(r/c)]}}{4\pi}\left(\frac{j\omega}{cr} + \frac{1}{r^2}\right) \quad (3.14)$$

Thus, the fields from the dipole have only three components $E_r, E_\theta \; and \; H_\varphi$. The components $E\varphi, Hr \; and \; H_\theta$ are everywhere zero, when r is very large, the terms in

$\frac{1}{r^2}$and $\frac{1}{r^3}$in (3.11), (3.12) and (3.14) can be

neglected in favor of the terms in 1/r.
Thus, in the **far field**, $E_r$is negligible, and we have effectively only two field components, Electric (E_Θ) and Magnetic field ($H\varphi$), given by

$$E_\theta = \frac{I_0 L \cos\theta \, e^{j\omega\left[t-\left(\frac{r}{c}\right)\right]}}{4\pi\varepsilon_0 c^2 r} = \boldsymbol{j\frac{I_0 \beta L}{4\pi\varepsilon_0 cr}\sin\theta e^{j\omega[t-(r/c)]}} \quad (3.15)$$

$$H_\phi = \frac{j\omega I_0 L \sin\theta e^{j\omega\left[t-\left(\frac{r}{c}\right)\right]}}{4\pi cr} = \boldsymbol{j\frac{I_0 \beta L}{4\pi r}\sin\theta e^{j\omega[t-(r/c)]}} \quad (3.16)$$

Also, the impedance of the space can be calculated as;

$$\frac{E_\theta}{H_\phi} = \sqrt{\frac{\mu_0}{\varepsilon_0}} = 377\Omega.$$

At low frequencies the Electric and Magnetic fields are derived,

$$[I] = I_{0e}{}^{j\omega[t-(r/c)]} = j\omega[q] \quad (3.17)$$

Therefore, E_r and E_θ can be written as;

$$\boldsymbol{E_r} = \frac{[q]\boldsymbol{L}\cos\boldsymbol{\theta}}{2\pi\varepsilon_0}\left(\frac{j\omega}{cr^2} + \frac{1}{r^3}\right) \quad (3.18)$$

and

$$\boldsymbol{E_\theta} = \frac{[q]\boldsymbol{L}\cos\boldsymbol{\theta}}{4\pi\varepsilon_0}\left(\frac{\omega^2}{C^2 r} + \frac{j\omega}{Cr^3} + \frac{1}{r^3}\right) \quad (3.19)$$

While the magnetic field (H_φ) is given as

$$\boldsymbol{H_\phi} = \frac{[I]\boldsymbol{L}\cos\boldsymbol{\theta}}{4\pi}\left(\frac{j\omega}{Cr} + \frac{1}{r^2}\right) \quad (3.20)$$

At low frequencies, ω approaches zero so that the terms with ω *in the* numerator can be neglected. As $\omega \rightarrow 0$. We also have

$$[q] = q_0 e^{j\omega[t-(r/c)]} = q_0 \quad (3.21)$$

and

$$[I] = I_0 \quad (3.22)$$

Therefore, the field components would be given as;

$$\boldsymbol{E_r} = \frac{q_0 \boldsymbol{L}\cos\boldsymbol{\theta}}{2\pi\varepsilon_0 r^3} \quad (3.23)$$

$$\boldsymbol{E_\theta} = \frac{q_0 \boldsymbol{L}\sin\boldsymbol{\theta}}{4\pi\varepsilon_0 r^3} \quad (3.24)$$

$$\boldsymbol{H_\phi} = \frac{I_0 \boldsymbol{L}\sin\boldsymbol{\theta}}{4\pi r^2} \quad (3.25)$$

NB: E_r = Electric field in r-direction
E_θ= Electric field in θ-direction
H_ϕ = Magnetic field in ϕ-direction
L = Length of dipole
q_0= charge
r = distance from the radiating source
c = velocity of light = $3*10^8$m/s
μ_0 = permeability of free space
($4\pi \times 10^{-7}$H m^{-1})

4 RESULTS

The results of simulating the relationship between magnetic and electric fields with distance using JupyterNoteBook are shown in Figures 4 and 5. It shows that as the field's distance from the radiating source increases, both the magnetic and electrical fields gradually decrease.

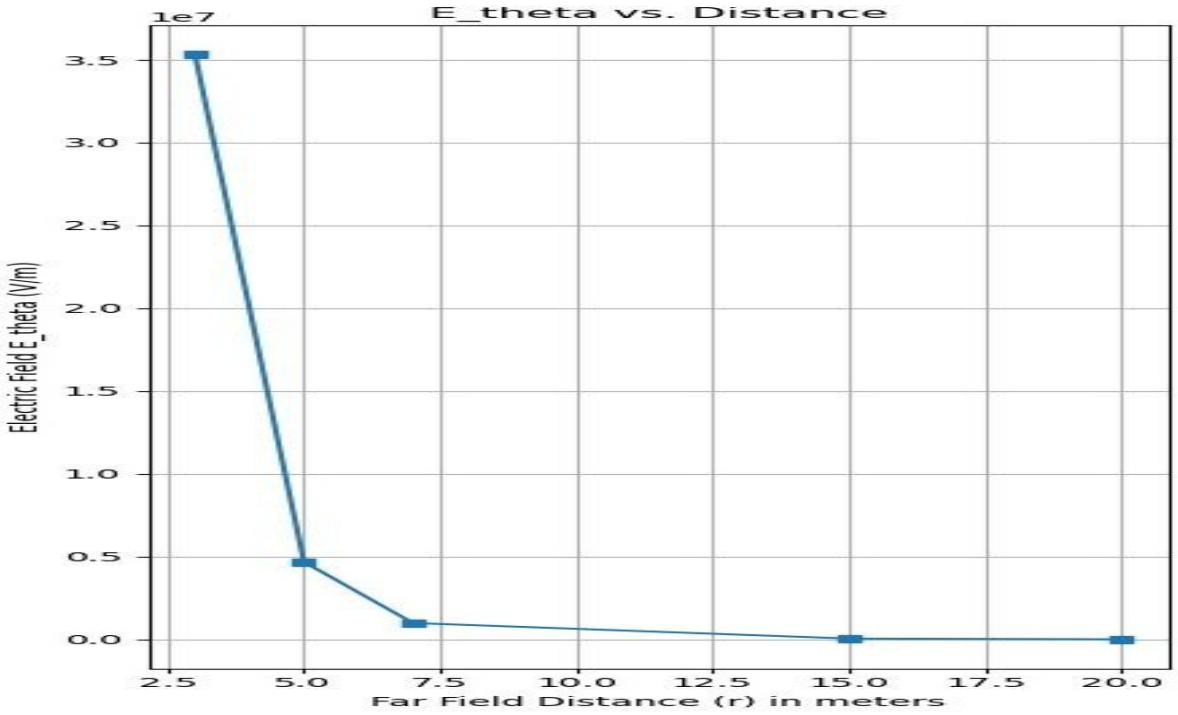

Fig.4: Simulations of Electric field in θ -direction (E_θ) against far field distance

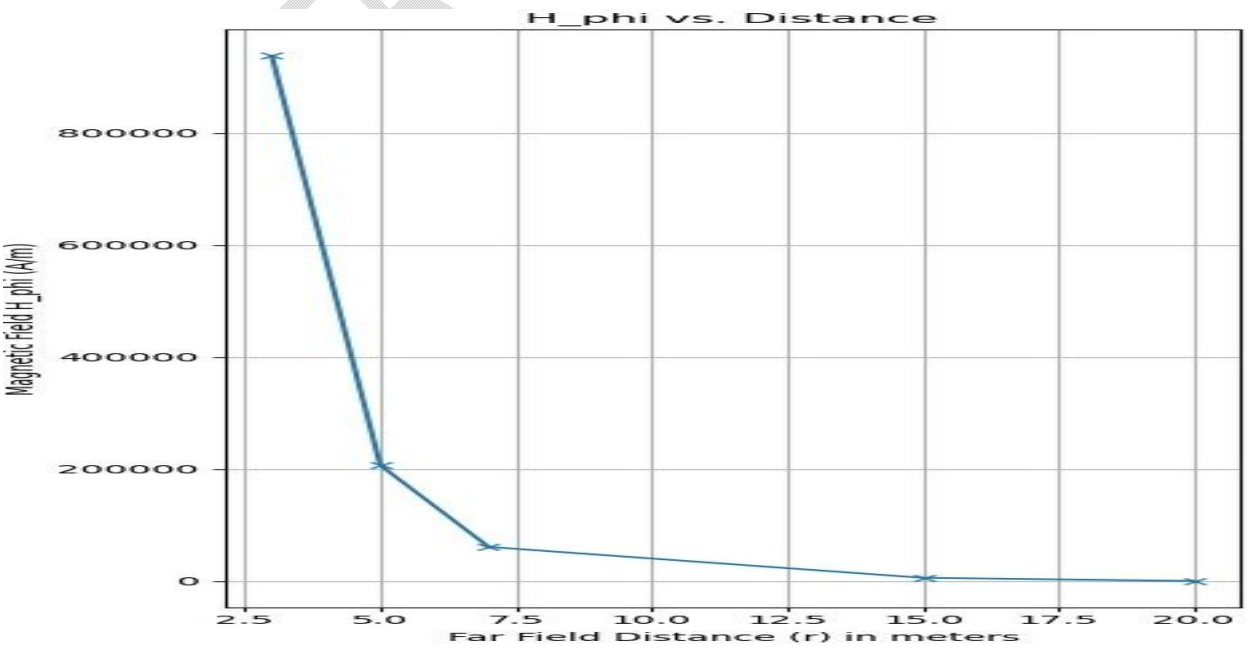

Fig.5: Simulation of Magnetic field in ϕ- direction (H_ϕ) against the field distance

The figures 6 and 7 are results of electric and magnetic field obtained through simulations with phase angles. It shows a sinusoidal wave characteristic for both fields. It is observed that both Electric and Magnetic fields are maximum between 75 and 100 degree phase angle.

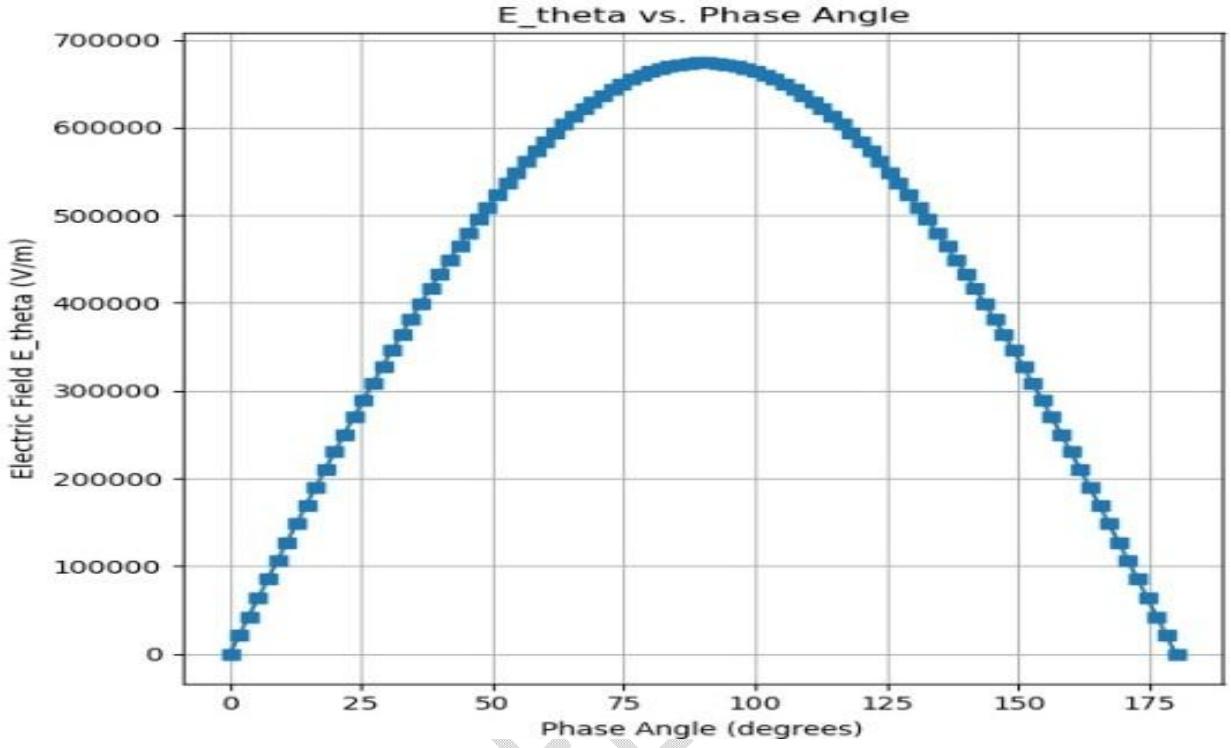

Fig.6: Simulated result of Electric field in θ- direction (E_θ) against Phase Angle

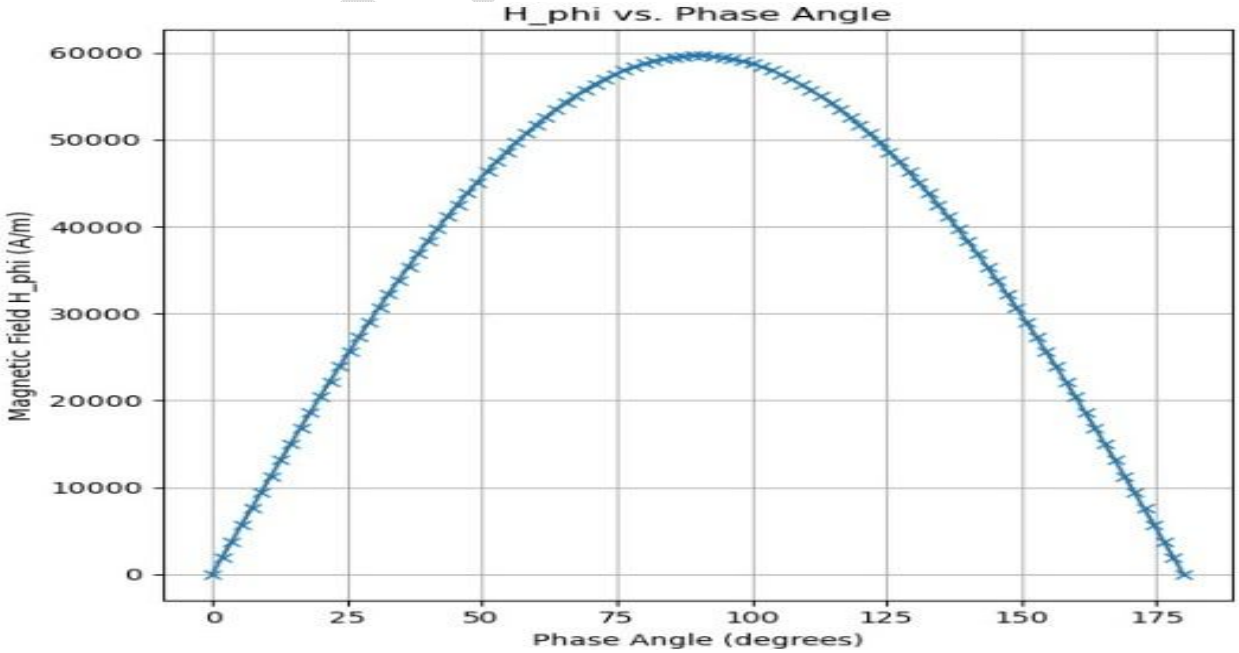

Fig.7: Simulated result of Magnetic field in ϕ-direction (H_ϕ) against Phase Angle

Figures 8 and 9 shows simulated results of electric and magnetic fields at low frequencies.

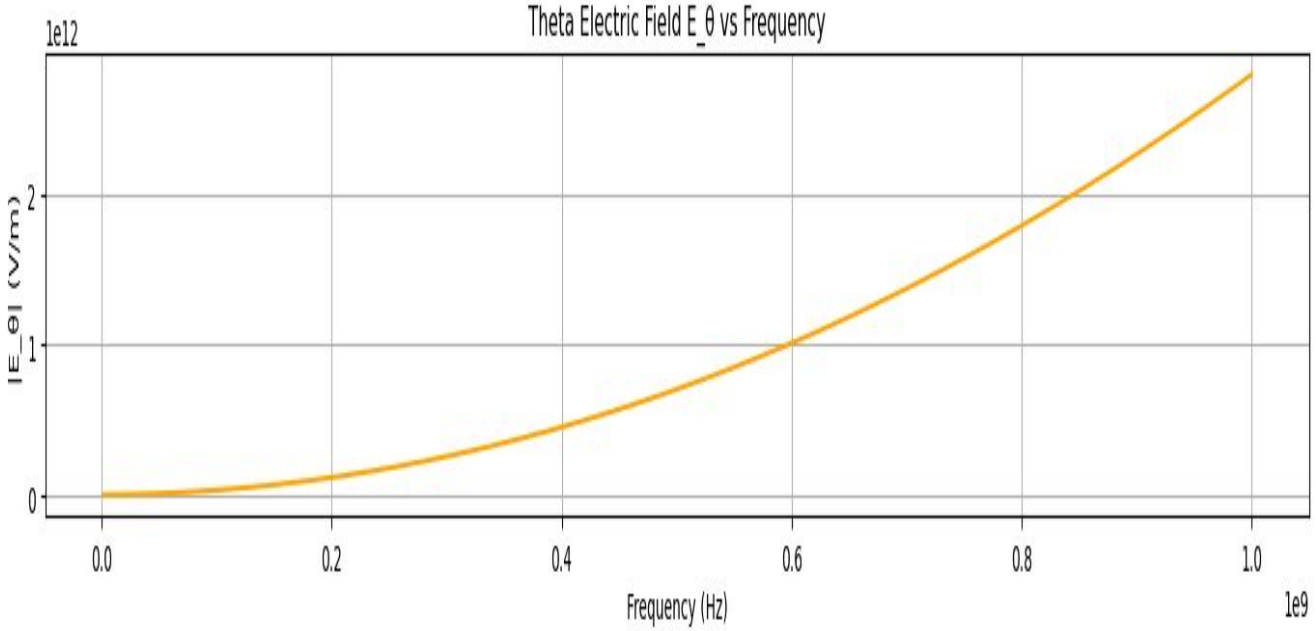

Fig.8: Simulated result of Electric field in θ- direction (E_θ) against frequency

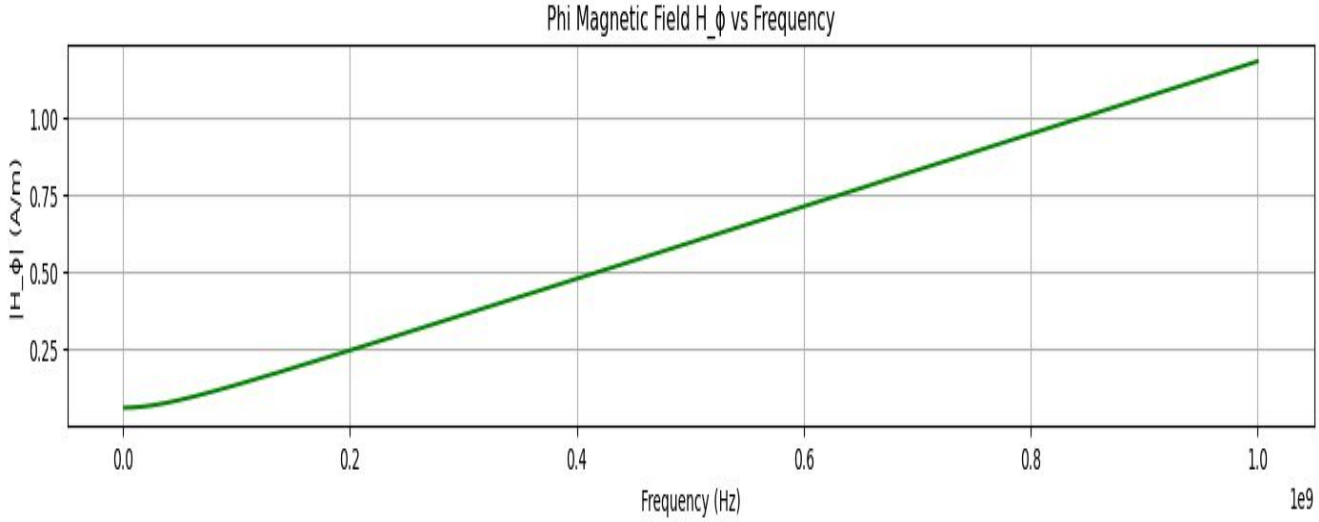

Fig.9: Simulated result of Magnetic field in ϕ-direction (H_ϕ) against frequency

Figure 10 is the result of the electric field characteristics with the length of the dipole antenna. It shows a straight-line relationship.

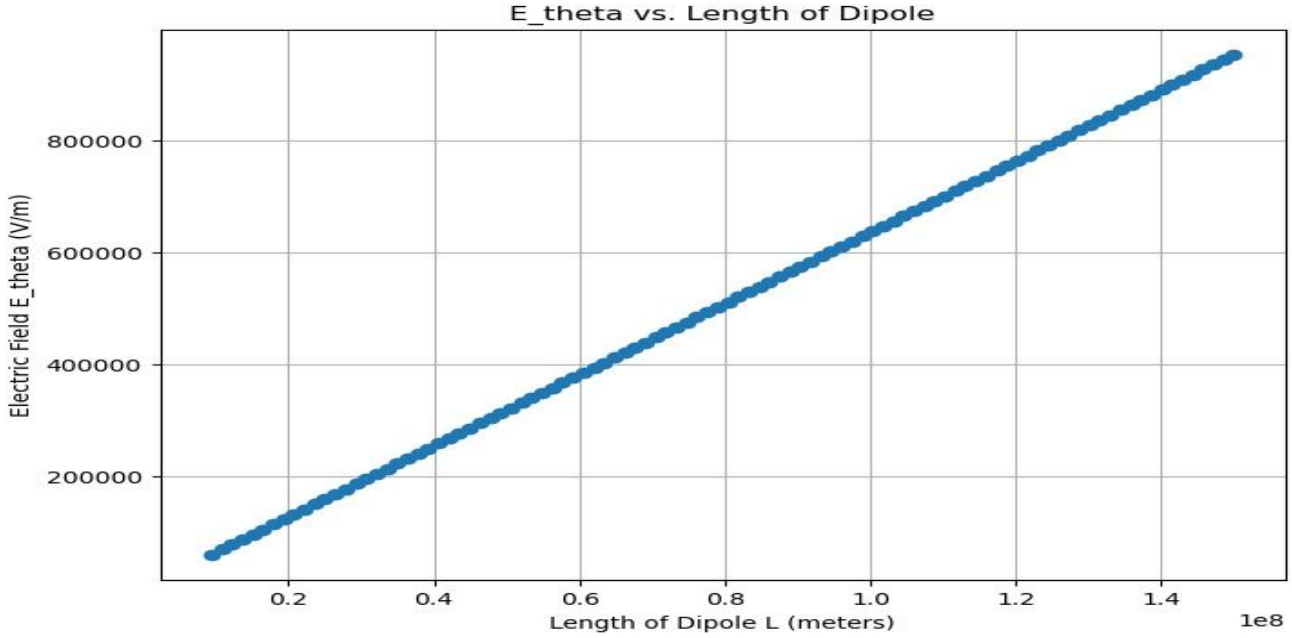

Fig.10: Simulated result of Electric field in θ- direction (E_θ) against Dipole length

Figures 11, 12, 13 and 14 are the radiation pattern of dipole antenna at low frequencies obtained after simulations.

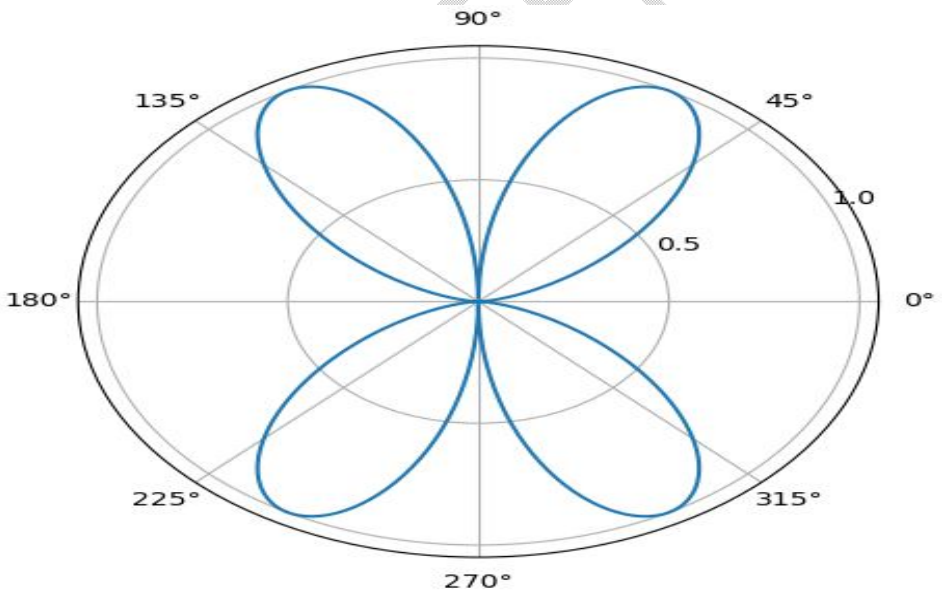

Fig. 11: Far field radiation pattern frequency = 1KHz, wavelength= 300,000m

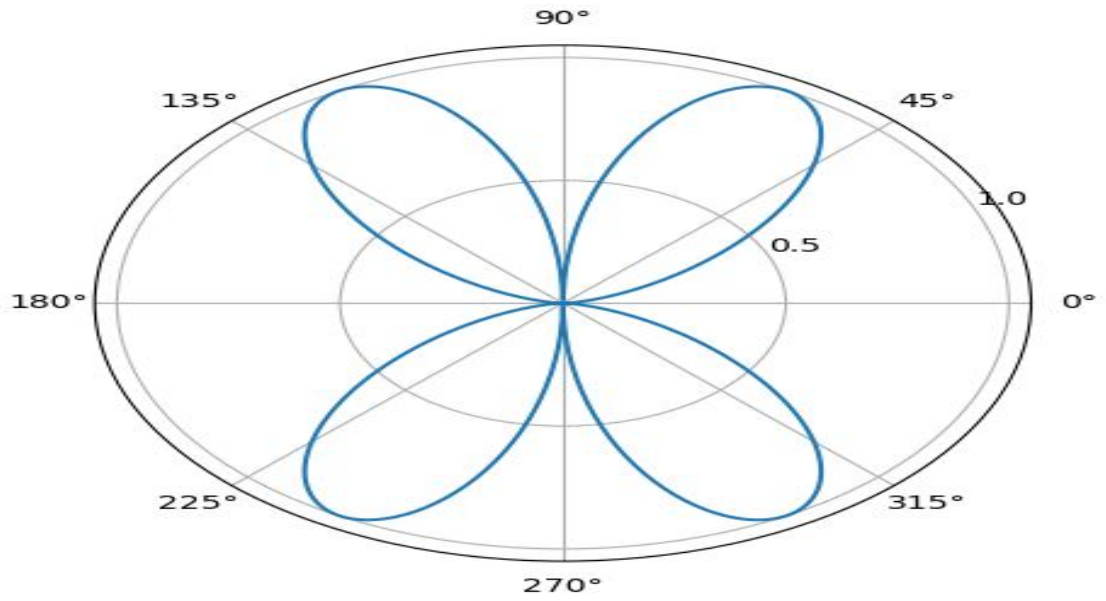

Fig. 12: Far field radiation pattern frequency = 3KHz, wavelength= 100,000m

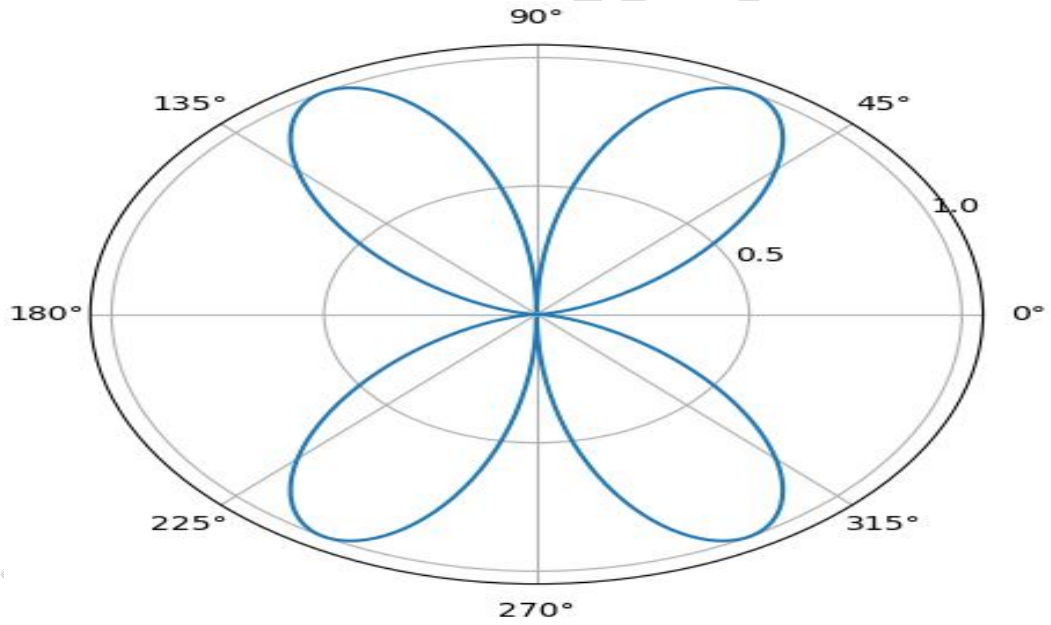

Fig. 13: Far field radiation pattern frequency = 5KHz, wavelength= 60,000m

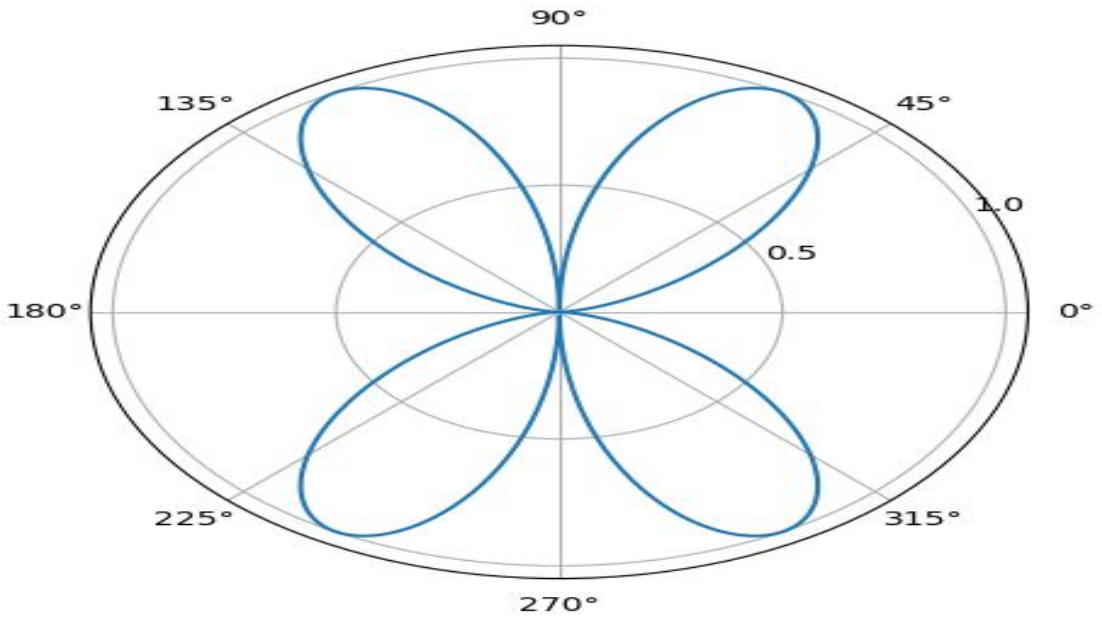

Fig. 14: Far field radiation pattern frequency = 7KHz, wavelength= 4285.14m

5 DISCUSSION

The simulated results of the electric (Eθ) and magnetic field (Hϕ) model from the dipole antenna's far field region are shown in Figures 4 and 5. The data indicate that the electric and magnetic fields have their maximum values at the closest distance from the source, but that they gradually drop as one moves farther away.

The electric field (Eθ)) and magnetic field (Hϕ) components in Figures 6 and 7 exhibit a sinusoidal variation that aligns with the oscillation of the wave. The amplitudes of the magnetic and electric fields are, respectively, 60000 A/m and 680,000 V/m. This outcome demonstrates the electric and magnetic fields' sinusoidal character and how it relates to phase angle, and are maximum between 75 and 100 degrees phase angle.

The magnetic field and electric field components in the phi- and theta-directions (Eθ and Hϕ, respectively), against low frequencies in the far-field region are shown in Figures 8 and 9, which shed light on how electromagnetic waves behave at lower frequencies. The electromagnetic wave's wavelength lengthens at low frequencies, causing the far-field zone to begin farther away from the source. Er is still very small, but because of wider radiation patterns and reduced antenna efficiency, Eθ and Hϕ are trending downward.

The simulated findings of the association between the dipole antenna's length and the theta-direction electric field (Eθ) are displayed in figure 10. The outcome demonstrates that the electric field's strength in the theta direction increases as the dipole's length does.The electric field (Eθ), which reflects variations in the radiation pattern and efficiency of the antenna, varies dramatically with dipole length. Plotting 0 for magnetic field means that, given a perfect dipole oriented along the z-axis, magnetic field (Hu) stays zero.

The dipole antenna's far field radiation is seen in Figures 11–14. When 1 kHz, 3 kHz, 5 kHz, and 7 kHz were taken into consideration, the wavelength grew significantly. The wavelength for a 1 KHz frequency was 300,000 meters. The dipole operates similarly throughout these low frequencies when the wavelength is significantly more than the antenna's physical dimensions. An almost equal current distribution follows the antenna elements, producing a radiation pattern that is comparable.

6 CONCLUSION

The model, simulations of the magnetic, electric, and far-field radiation patterns of a dipole antenna at low frequencies have all been presented in this study. Understanding the relationships between the electric field (Er), magnetic field (Hυ), distance (r), frequency (f), and phase angle (υ) might help one better comprehend how a short dipole antenna propagates waves. It was also noted that the radial component of the electric field (Er) usually becomes minimal (nearly zero) in the far-field region in comparison to the transverse components (Eθ) and (Hϕ). This is due to the fact that the electric and magnetic fields are perpendicular to the direction of propagation in a far-field wave, which is primarily transverse.

Thus, a deeper comprehension of the correlation between the electric or magnetic field and the dipole length, phase angle, distance, or frequency leads to a better grasp of the properties of microwave propagation. In order to maximize signal strength and reach, low-frequency communication systems—like AM radio and some military communication systems—benefit from an awareness of these electric field changes. Furthermore, this approach is essential to comprehending the design and performance optimization of dipole antennas.

REFERENCES

1. M. Ramakrishna and D. Reddy, “IOT Based Digital Notice Board,” Mar. 2017.

2. V. Ravi Sekhara Reddy, B. V. Naga Sai, N. Venkata Pavan Kumar, S. Sai Vardhan Reddy, and B. Sai Kathyayani, “Design of dipole aerial by using COMSOL multi physics software,” Mater. Today Proc., vol.80, pp. 3481–3485, 2023, doi: 10.1016/j.matpr.2021.07.278.

3. S. Hashemi, “Dipole Antenna Based on Forward-Coupling Multilayer Ring Resonators (MRR),” 2019 IEEE 19th Mediterr. Microw. Symp. MMS, pp. 1–4, Oct. 2019,
doi: 10.1109/MMS48040.2019.9157254.

4. M. M. Mansour, K. S. Sultan, and H. Kanaya, “High-Gain Simple Printed Dipole-Loop Antenna for RF-Energy Harvesting Applications,” 2020 IEEE Int. Symp. Antennas Propag. North Am. Radio Sci. Meet., pp. 1441–1442, Jul. 2020, doi: 10.1109/IEEECONF35879.2020.9329835.

5. G. Jin, C. Deng, Y. Xu, J. Yang, and S. Liao, “Differential Frequency-Reconfigurable Antenna Based on Dipoles for Sub-6 GHz 5sG and WLAN Applications,” IEEE Antennas Wirel. Propag. Lett., vol. 19, no. 3, pp. 472–476, Mar. 2020,
doi: 10.1109/LAWP.2020.2966861.

8. Suraya M, Anusha, SAMATHA .S, Mounika .D, (2017): Design of Dipole Antenna and various radiation patterns for various lengths.

9. G. Mansour, E. Nugoolcharoenlap, and F. Shkal, “Broadband Printed Dipole Array Antennas,” 2023 IEEE 3rd Int. Maghreb Meet. Conf. Sci. Tech. Autom. Control Comput. Eng. MI-STA, pp. 623–627, May 2023, doi: 10.1109/MI-STA57575.2023.
10169392.

10. N. Abdul Malek, R. D. Seager, J. A. Flint, and Z. Zainal Abidin, “Analysis, Optimization, and Hardware Implementation of Dipole Antenna Array for Wireless Applications,” Int. J. Antennas Propag., vol. 2022, pp. 1–14, Aug. 2022, doi: 10.1155/2022/1741454.

11. M. S. Miah, M. Heino, C. Icheln, and K. Haneda, “Design of a Reference Dipole-Loop Antenna Array at 28 GHz,” 2019 13th Eur. Conf. Antennas Propag. EuCAP, Mar. 2019, Accessed: Apr. 30, 2024. [Online]. Available: https://www.semanticscholar.org/paper/Design-of-a-Reference-Dipole-Loop-Antenna-Array-at-Miah-eino/d4c2f6209d434a63741
2325963cae0df14c981ac

12. S. Varma, S. Sharma, M. John, R. Bharadwaj, A. Dhawan, and S. K. Koul, “Design and Performance Analysis of Compact Wearable Textile Antennas for IoT and Body-Centric Communication Applications,” Int. J. Antennas Propagation., vol. 2021, pp. 1–12, Aug. 2021, doi:10.1155/2021/7698765.

13. Cai, Z. Weng, Y. Qi, J. Fan, and W. Zhuang, “A High-Performance Standard Dipole Antenna Suitable for Antenna Calibration,” IEEE Trans. Antennas Propag., vol. 69, no. 12, pp. 8878–8883, Dec. 2021, doi: 10.1109/TAP.2021.3091637.

14. O. Sanusi, L. Roy, Y. Wang, and F. Ghaffar, “Impact of Blood Environment on Integrated Antenna Performance,” 2020 Int. Appl. Comput. Electromagn. Soc. Symp. ACES, pp. 1–2, Jul. 2020, doi: 10.23919/ACES49320.2020.9196099.

15. F. Benmahmoud, P. Lemaitre-Auger, and S. Tedjini, “Wearable Folded Planar Dipole Antenna: Design and assessment for on-body wireless communication devices,” IEEE Antennas Propag. Mag., vol. 65, no. 1, pp. 27–39, Feb. 2023.
doi:10.1109/MAP.2022.3216783.

16. S. Chen, X. Shi, Y. Yao, Y. Gao, and Y. Yuan, “Enhanced Transmission Performance of a Dipole Antenna Based on a Ceramic Diamond-Structure PBG Substrate with a Defect Cavity,” J. Electron. Mater., vol. 49, no. 9, pp. 5363–5367, Sep. 2020,
doi:10.1007/s11664-020-08269-6.

17. P. M. Neelamraju, P. Pothapragada, G. Rana, D. Chaturvedi, and R. Kumar, “Machine Learning based Low-Scale Dipole Antenna Optimization using Bootstrap Aggregation,” 2023 2nd Int. Conf. Paradigm Shifts Commun. Embed. Syst. Mach. Learn. Signal Process. PCEMS, pp. 1–4, Apr. 2023, doi:10.1109/PCEMS58491.2023.10136108.

18. H. Aliakbari and B. Lau, “Characteristic Mode Analysis of Planar Dipole Antennas,” 2019 13th Eur. Conf. Antennas Propag. EuCAP, Mar. 2019, Accessed: Apr. 30, 2024. [Online]. Available: https://www.semanticscholar.org/paper/Characteristic-Mode-Analysis-of-Planar-Dipole-Aliakbari Lau/e7dcb1631bad6e8639af444f3152a617ffb4e3a4